

A Fully Electronic System for the Time Magnification of Ultra-Wideband Signals

Joshua D. Schwartz, *Student Member, IEEE*, José Azaña, *Member, IEEE*, and David V. Plant, *Senior Member, IEEE*

Abstract—We present the first experimental demonstration of a fully electronic system for the temporal magnification of signals in the ultra-wideband regime. The system employs a broadband analog multiplier and uses chirped electromagnetic-bandgap structures in microstrip technology to provide the required signal dispersion. The demonstrated system achieves a time-magnification factor of five in operation on a 0.6-ns time-windowed input signal with up to 8-GHz bandwidth. We discuss the advantages and limitations of this technique in comparison to recent demonstrations involving optical components.

Index Terms—Analog multipliers, frequency conversion, microstrip filters, signal detection, signal processing.

I. INTRODUCTION

THE increasing attractiveness of ultra-wideband (UWB) communication, in the context of both short-range wireless and long-range radar and imaging systems, has spurred research towards updating conventional signal-processing systems to accommodate the characteristically large bandwidths of UWB pulses, which span several gigahertz. These bandwidths generally surpass the capabilities of current instrumentation for analog-to-digital conversion (ADC) and arbitrary waveform generation (AWG), both of which represent key signal-processing tools in the development of UWB systems [1]–[5]. Temporal imaging or “time-stretch” systems, in which arbitrarily shaped time-limited input signals can be distortionlessly magnified, compressed, or reversed in the time domain, are capable of extending the operating bandwidths of existing ADC and AWG systems by adding a bandwidth-conversion step, as illustrated in Fig. 1. Temporally magnifying (i.e., stretching) an analog UWB input signal prior to ADC would permit the sampling of the signal to be performed at a relaxed rate without losing information [1], [2]. Similarly, in the context of AWG, introducing a time-compression block at the system output would compress the generated waveforms to bandwidths of interest for UWB communication beyond the capabilities of current AWG implementations, which are limited at 2 GHz [4], [5].

Manuscript received August 8, 2006; revised October 24, 2006. This work was supported in part by the Natural Sciences and Engineering Research Council of Canada.

J. D. Schwartz and D. V. Plant are with the Photonics Systems Group, Department of Electrical and Computer Engineering, McGill University, Montréal, QC, Canada H3A 2A7 (e-mail: joshua.schwartz@mcgill.ca).

J. Azaña is with the Institut National de la Recherche Scientifique-Energie, Matériaux et Télécommunications, Montréal, QC, Canada H5A 1K6 (e-mail: azana@emt.inrs.ca).

Color versions of one or more of the figures in this paper are available online at <http://ieeexplore.ieee.org>.

Digital Object Identifier 10.1109/TMTT.2006.890069

Recent demonstrations of time-stretching systems intended for the aforementioned microwave applications have almost exclusively invoked the optical domain [1]–[5]. This presents a problem for microwave systems from an integration standpoint, as signal conversion to and from the optical domain necessitates the cumbersome element of electrooptic modulation, and the referenced works require costly mode-locked or supercontinuum laser sources.

The decision to perform time-stretching operations in the optical domain was motivated in part by a perceived lack of a sufficiently broadband low-loss dispersive element in the electrical domain such as that which is readily available in optical fiber [2]. In our recent study [6], we proposed a fully electronic implementation for a time-magnification system by using chirped electromagnetic-bandgap (EBG) structures in microstrip technology as a source of broadband dispersion. Here, we present the first experimental demonstration of a working $5\times$ time-magnification system for signals with bandwidths of several gigahertz. We also discuss the capabilities and limitations of fully electronic time-stretch systems, as compared to their optically implemented counterparts, and we investigate timing and system resolution issues.

This paper is organized as follows. In Section II, we provide a very brief review of the theory of time-stretch systems before discussing, in Section III, the measured performance of our time-magnification system. Section IV details some of the challenges and limitations associated with purely electronic time-stretch systems, paying particular attention to how they compare to electrooptic implementations.

II. BACKGROUND

The theory of time stretching originated in the work of Caputi [7] and can be understood in the context of an elegant space–time duality between the paraxial diffraction of a propagating wave in space and the narrowband dispersion of a propagating wave in time, which share a common mathematical framework [8]–[10]. As a result of this duality, the traditional spatial imaging system consisting of a thin lens between two diffractive media (such as air) has an analog in the time domain, which consists of a “time lens” between two dispersive media. The function of the “time lens” is to emulate in the time domain the effect that a thin curved lens surface has in space on a propagating wave: namely, quadratic phase modulation. Whereas a space-lens introduces into a z -propagating wave a phase term quadratically related to spatial x – y coordinates, a “time lens” introduces into a propagating wave a quadratic-phase term in the time domain. This can be achieved in electronics

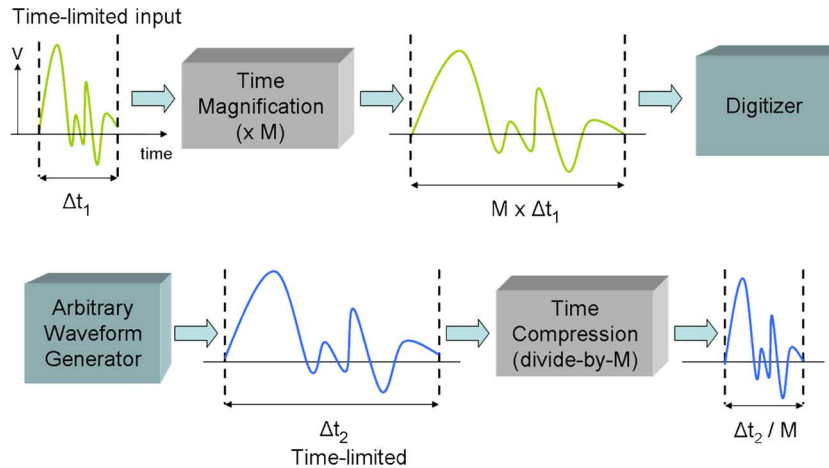


Fig. 1. Conceptual illustration of the application of time stretching. Time magnification facilitates ADC by reducing the frequency and bandwidth of the input signal (*top*), while time compression enables high-frequency AWG by frequency upshifting the generated waveform (*bottom*).

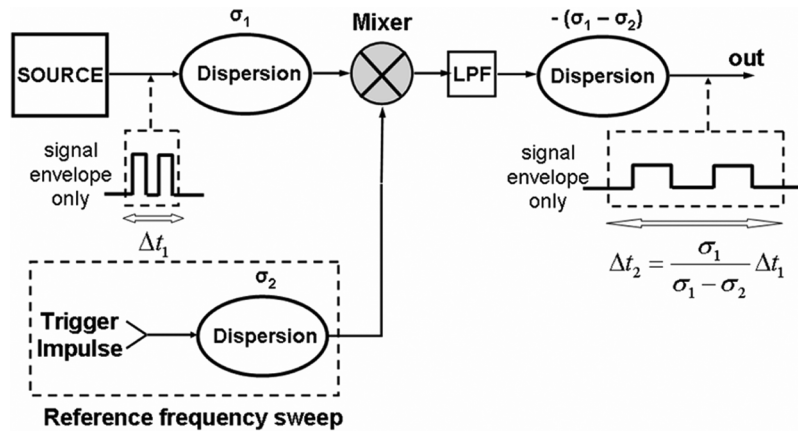


Fig. 2. Schematic representation of a time-stretch system. Reference linear frequency sweep is shown generated passively. An LPF is employed to select the difference-frequency product of the mixing operation.

by mixing a signal against a linear frequency ramp, which is straightforward to implement using an analog multiplier.

A schematic depiction of time stretching is presented in Fig. 2. An input signal of carrier frequency ω_0 , bandwidth $\Delta\omega_1$, and constrained to time-window Δt_1 is passed through a dispersive element with linear group delay of slope σ_1 (nanoseconds/gigahertz). Given a value of σ_1 satisfying the condition

$$\left| \frac{\Delta t_1^2}{4\sigma_1} \right| < 1 \quad (1)$$

this dispersion is sufficient to perform a frequency-to-time mapping of the signal, ordering the spectral components [11]. The dispersed signal is then difference-frequency¹ mixed against a linear frequency sweep of slope σ_2 , shown generated in Fig. 2 by a passive process: applying dispersion to an impulse. The resulting product has a reduced central frequency ω_{0_out} , a new group-delay slope $\sigma_3 = (\sigma_1^{-1} - \sigma_2^{-1})^{-1}$, and the bandwidth is

¹In this discussion, we neglect the sum-frequency components of the mixing operation, as these can be easily filtered out. It is possible to perform time stretching using the sum frequencies instead, and the decision rests upon the available operation bandwidth of the output dispersive network or on the choice of a magnifying or compressing system [12].

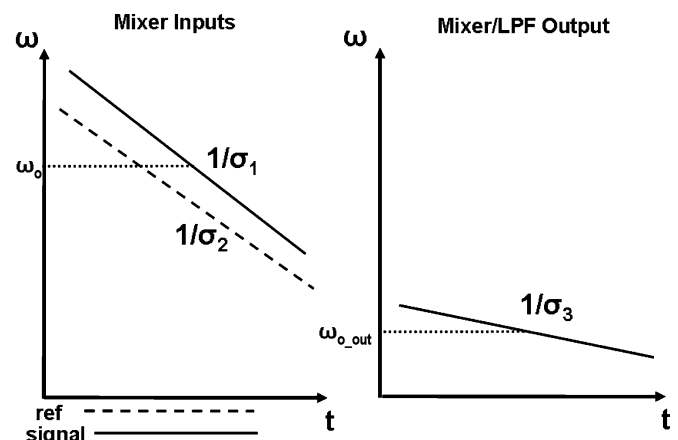


Fig. 3. Frequency-time representation of dispersed input signal and reference impulse (frequency sweep), as well as difference-frequency mixer output.

reduced in this step in proportion to the ratio σ_1/σ_3 while the signal remains the same duration in time. A frequency-time representation of this mixing process is illustrated in Fig. 3, valid if (1) is respected. If this signal is then compressed (i.e., dispersed with group-delay slope $-\sigma_3$), the original input signal

TABLE I
COMPARISON OF COMMONLY CHIRPED STRUCTURES

Device/Criteria	Medium	Typical Delay Slopes	Typical Bandwidths (center frequency)	Dimensions	Typical Insertion Loss
Chirped Fiber Bragg Grating	Optical	100 ps / nm	THz (optical regime - hundreds of THz)	~10 cm / ns delay	~ 3 dB (includes optical circulator)
Chirped Surface Acoustic Wave	Electrical / Acoustic	10 – 40 μ s / MHz	Up to ~ 1 GHz (~ 1 GHz)	1-2 mm ²	~ 20 dB
Chirped EBG	Electrical	0.1-2 ns / GHz	Up to 15 GHz (5 - 15 GHz)	~10 cm / ns delay	~ 7 dB (includes 6 dB coupler)

can be recovered from the signal envelope, stretched temporally by the magnification factor $M = \sigma_3/\sigma_1$ and reduced in amplitude by the same factor, respecting conservation of energy (assuming lossless mixing and dispersion operations). For $|M| > 1$, magnification is achieved, while $|M| < 1$ indicates time compression and $M < 0$ has the effect of time reversing the signal. It should be noted that the output signal is effectively an amplitude modulation on a chirped carrier corresponding to the difference-frequency band created in the mixing process, and must still be envelope detected somehow to recover signal information.

III. EXPERIMENTAL DEMONSTRATION

The authors proposed and simulated an electronic time-magnification system in [6] and here present the first experimental demonstration of such a system intended for use at bandwidths of interest to UWB communication systems. We have found that the dispersive requirements of time-stretch systems can be met in the electrical domain by using chirped EBG structures, which were recently introduced in planar microstrip technology [13]. A reflective bandgap can be created in a microstrip line by “wiggling” the strip width in a sinusoidal fashion to induce Bragg-like local reflections, where the propagating wave is coupled to the same, but counter-propagating mode, and is reflected. Introducing a linear frequency chirp into the structure is accomplished by changing the period of the strip-width modulation along the length of the device, thus reflecting different frequencies at different lengths along the microstrip, yielding a linear group-delay slope (dispersion). These devices are similar to chirped fiber Bragg gratings in the optical domain, and chirped surface acoustic wave (SAW) structures common to radar, although they are far less lossy and easily achieve greater bandwidths than their SAW counterparts, as summarized in Table I.

A photograph of an etched 28-cm chirped EBG microstrip designed for operation between 2–10 GHz is shown in Fig. 4. This microstrip was meandered to fit into a 10-cm² etching process, though the radius of curvature and the strip spacing were designed to exhibit negligible radiative and cross-coupling effects.

To generate the reference frequency sweep, we employed a passive-generation scheme, as proposed in Caputi’s original system, and in a manner similar to the recent optical time-stretch system schemes using dispersed ultra-short optical pulses [1]–[3]. Actively generating a frequency ramp spanning up to 8 GHz at a sweep rate of several gigahertz/nanosecond is prohibitively difficult, and there exists, to the authors’ knowledge, no suitable voltage-controlled oscillator for this purpose that is commercially available. A Picosecond Pulse

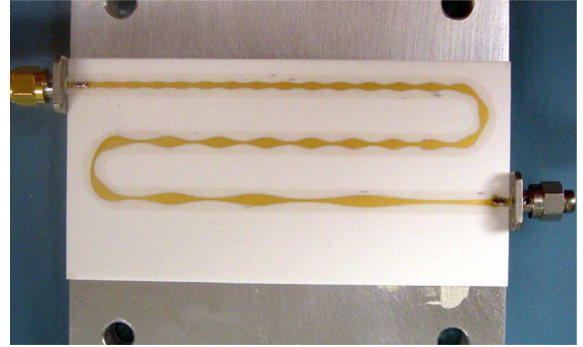


Fig. 4. From [6]. Photograph of the 28-cm chirped EBG microstrip used in the demonstration. Microstrip is gold metallized on an alumina substrate and is meandered to fit a 10-cm² etching process.

Labs model 3600 impulse generator was used to create a train of -7.5 -V 70-ps impulses to provide useful bandwidth out to 10 GHz. These impulses were dispersed using a chirped EBG microstrip, resulting in a linear frequency sweep. Ideally, this sweep would exhibit a flat-amplitude response since the goal is to have a difference-frequency mixing product that contains only those amplitude features belonging to the RF input signal. Unfortunately, a dispersed impulse will feature amplitude rolloff associated with its spectral content with diminished amplitude towards the higher frequencies. However, since this rolloff represents *a priori* information, its effect on signal measurements can be compensated for in post-process as needed.

Our demonstration system employs three chirped microstrip EBG designs (wherever dispersion is indicated in Fig. 1). We selected Coorstek’s ADS-96R substrate for these microstrips (1.27-mm thickness, $\epsilon_r = 9.41$, $\tan \delta = 0.0007@10$ GHz). The EBGs were designed to have group-delay slopes $\sigma_1 = -0.4$ ns/GHz, $\sigma_2 = -0.5$ ns/GHz, and $-\sigma_3 = +2$ ns/GHz for the input dispersive network, reference frequency-sweep generator, and output compressing network, respectively, where we note the change in sign of the group-delay slope of the third (compressive) EBG structure. The system magnification factor $M = \sigma_3/\sigma_1$ was designed to be +5, while the slope required of the reference frequency sweep was determined according to [7] as

$$\sigma_2 = \left(\frac{1}{\sigma_1} - \frac{1}{\sigma_3} \right)^{-1}. \quad (2)$$

The input and reference-sweep microstrips both operated in the band of 2–10 GHz and were 28 cm in length, while the output compressive network was designed for operation from 1–2.5 GHz and was 38 cm in order to have enough periods at

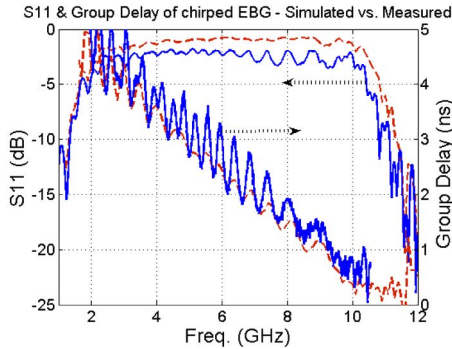


Fig. 5. Simulated (dashed line) and measured (solid line) S_{11} and group delay (reflected port) of the photographed microstrip of Fig. 4. The group-delay slope is approximately -0.5 ns/GHz. Loss is somewhat higher in measurement (2–3 dB) due to end connectorization impedance mismatching, which also worsens the measured group-delay ripple by contributing to long-path resonances.

these low frequencies to induce reflection. The microstrips were designed according to the empirical formula proposed in [13]

$$Z_o(z) = 50 \cdot \exp \left(A \cdot W(z) \cdot \sin \left(\frac{2\pi}{a_o} \cdot z + C \cdot \left(z^2 - \frac{L^2}{4} \right) \right) \right). \quad (3)$$

This expression yields an impedance modulation centered around 50Ω —in our case, this impedance varied from 35 to 65Ω at the widest and narrowest points of the strip, respectively. The microstrip is of length L , local period “ a_o ” at the center of the structure ($z = 0$), and a chirp C (m^{-2}), which is related to the target group-delay slope σ (nanoseconds/gigahertz) by

$$C = \frac{4\pi}{\sigma} \cdot \left(\frac{\sqrt{\epsilon_{\text{eff}}}}{c} \right)^2. \quad (4)$$

Here, ϵ_{eff} is the effective permittivity of the microstrip. We employed in (3) an asymmetric Gaussian apodization window $W(z)$ to help flatten the response and increase the reflectivity of the EBG for the longer lossier round-trips of the lower frequencies. We refer the interested reader to [11] and [13] for further details concerning this procedure. Once fabricated, the microstrips were mounted on aluminum baseplates and end connectorized to subminiature A (SMA) connectors. Each microstrip was $50\text{-}\Omega$ terminated on the far end. The microstrips were then paired with an appropriate commercially available 6-dB directional coupler covering their bandwidths in order to circulate the reflected dispersed signals.

A sample of chirped EBG microstrip S_{11} and group-delay response are presented in Fig. 5, both from simulation using Agilent’s Momentum software (a method-of-moments tool for full-wave analysis), and measured using Agilent’s 8720ES 20-GHz vector network analyzer. This microstrip, chosen for use in the reference-frequency generation step, was designed for a group-delay slope of $\sigma_2 = -0.5$ ns/GHz. Chirped microstrip EBGs suffer from group-delay ripple (as do their optical counterparts) due to undesired multiple internal reflections (long-path Fabry–Perot resonances). Apodization techniques can be employed to help mitigate this and other effects, which contribute to overall aberration in the imaging system [14]. Our measured results feature a more pronounced ripple than

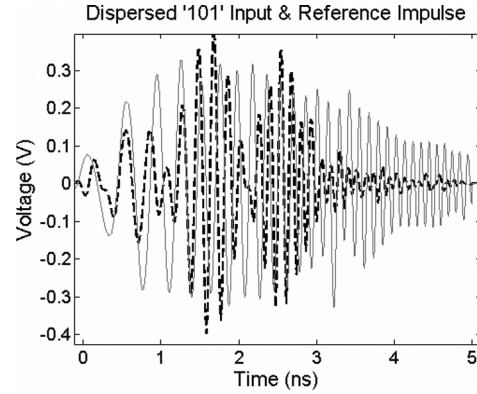


Fig. 6. MATLAB illustration of the “101” input signal centered at 5 GHz (dashed line) and the impulse (solid line) after they have undergone dispersion in chirped EBG microstrips. These are the inputs to the multiplier; their timing with respect to each other determines the output frequency difference.

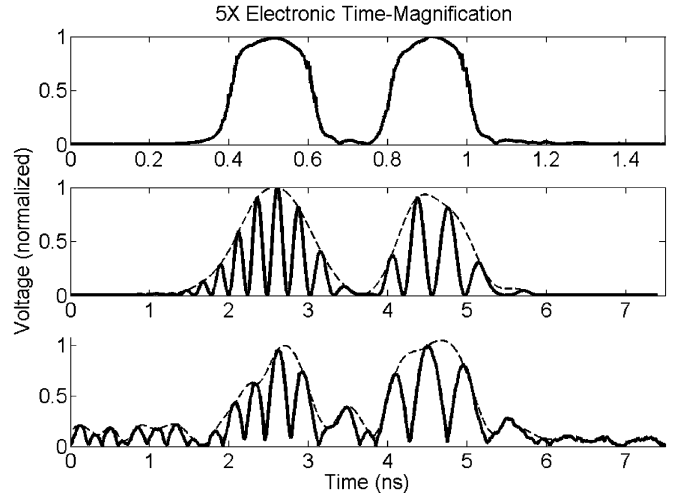


Fig. 7. 3-bit “101” test input at 5 Gb/s (top), shown from measurement before carrier modulation) and time-magnified outputs from simulation of the microstrips (middle) and from measurement (bottom). Outputs are normalized absolute values and have envelopes highlighted for visualization purposes.

simulations suggested, most likely due to the addition of reflections resulting from impedance mismatch at the soldered SMA end connectors; however, a measured group-delay slope of -0.506 ns/GHz was verified by smoothing this ripple using the averaging functions of the vector network analyzer.

The role of the “time lens” in our system was played by an analog multiplier (e.g., a Gilbert-cell architecture with predistortion circuitry), which can have very broad bandwidths through judicious choice of impedance-matching schemes [15], [16]. A differential multiplier topology was chosen to minimize noise effects and improve the conversion gain performance. The analog multiplier was fabricated in an available $0.5\text{-}\mu\text{m}$ SiGe BiCMOS technology and was simulated using the Cadence software suite. The design used a $+3.3\text{-V}$ supply and simple resistive networks for broadband impedance matching since power consumption was not a concern for this demonstration. We targeted a conversion gain of approximately 8 dB in the mixing process and employed an additional external amplifier at the output stage, which compensated for the anticipated

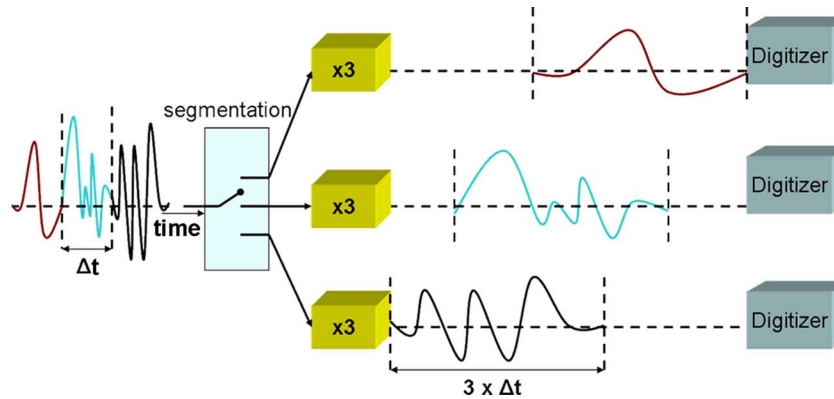


Fig. 8. Depiction of three parallel channels forming a free-running time-magnification front-end step for ADC.

losses associated with directional couplings and the time-magnification process itself. Input signals were brought on-chip using high-frequency probes from Cascade Microtech’s Infinity series, while a difference-frequency single-ended output of 1–2.5 GHz was passed off-chip via wirebond through the test board. The sum frequencies generated were inherently filtered, as they were attenuated by the test board, which effectively acted a low-pass filter (LPF) since the sum frequencies spanned 4.5–20 GHz.

For test inputs, the authors chose to work with differential digital bit-signaling for the ease with which windowing could be applied by strings of zeros, and since this is complicit with our system’s resolution limitations (see Section IV). For example, a simple 3-bit sequence “101” at 5 Gb/s and 2-V amplitude, generated differentially by an Anritsu MP1763B pulse pattern generator (PPG), fit within the target time window of 0.6 ns and was upconverted on a 5-GHz carrier using off-shelf diode mixers. Differential bit sequences were padded with zeros out to a 64-bit length and were sent through identical microstrip dispersion elements and couplers. The signal input and reference impulse, after dispersion in their respective chirped EBGs, were received by the analog multiplier. The impulse was triggered by a 1/64 clock output from the PPG and coarse timing adjustments were made by observing the multiplier output as different bits in the 64-bit stream were toggled to locate a nonzero product. In this fashion, the temporal alignment of the signal under test and the reference frequency sweep at the multiplier input could be verified.

An illustration of the post-dispersion signals being received by the multiplier is presented from measurement in Fig 6. These dispersed signals represent the spectral content of the RF input signal and impulse, ordered in the time domain, as described in [11] and subject to the 2–10-GHz bandpassing of the EBG microstrips. The amplitude of the dispersed reference impulse (solid trace) is nearly flat within the bandwidth of the input signal and, thus, post-processing was deemed unnecessary.

The multiplier product was compressed by the final EBG microstrip and a one-shot measurement was taken using a Tektronix CSA8000 scope with a 20-GHz electrical module. The result is illustrated in Fig. 7 in comparison to the (pre-carrier) “101” RF input, and also results predicted in [6] using the simulated microstrip S -parameters and ideal multiplication. No post-

processing has been applied to the measured signal, and the envelope is shown by interpolation (in MATLAB) for illustrative purposes. A time-scale factor of 5 has been applied to the time axis of the simulated and measured outputs to facilitate comparison. The “101” bit pattern is clearly distinguishable. Outputs have been normalized for clarity; the actual measured output amplitude was 140 mV at its peak after coupling/microstrip losses, time-magnification loss (a factor of 5) and the multiplier conversion gain of the system. It is clear that some distortion has taken place, which can be attributed to microstrip group-delay ripple (which shows up as an amplitude ripple) and also the frequency responses of the analog multiplier, directional couplers, and reference impulse, which are not flat.

IV. DISCUSSION

Here, we will discuss several challenges associated with implementing this system entirely in the electrical domain, particularly when contrasted with optical implementations.

A. Integrated Systems

Optical time-magnification systems have demonstrated time-apertures of approximately 2 ns [2], though because of (1) and because chirp cannot be increased indefinitely without paying a cost in the EBG reflectivity, it is clear that achieving larger time windows or even continuous operation would require segmenting and interleaving the input signal through parallel channels of operation [2]. Fig. 8 depicts what this would look like for a three-channel magnification system for an ADC application. This parallelization would be highly inconvenient in an optically enabled system, as it would require multiple electrooptic modulators and mode-locked lasers, which is cost prohibitive. By contrast, an electrical implementation requires several chirped microstrip EBGs, which are fairly long, but, being planar, can be stacked to conserve space. The authors suspect that a stripline-oriented EBG would be particularly convenient in a multiple metal-layer process. Parallelizing the system would also require several multiplier circuits and signal interleaving, which is straightforward and represents little overhead. One impulse generator, representing the most costly component, could still be employed by increasing its repetition rate and interleaving the impulses into each channel.

B. Time-Bandwidth Products and System Resolution

The input temporal aperture of a time-stretch system is intimately related to its bandwidth, and an appropriate figure-of-merit for a time-stretch system is the time-bandwidth product, defined as the product of the system's temporal aperture and its RF bandwidth, because of the implicit tradeoff between these two elements [2]. For the demonstrated system, this product is modest: approximately $0.6 \text{ ns} \times 8 \text{ GHz} \approx 5$, whereas demonstrations in the optical domain have been shown to achieve products as high as 60 [17]. Furthermore, the resolution of our demonstrated system is particularly limited because the electrical carrier frequency is so close to the bandwidth of the baseband RF signal. Systems employing photonic components benefit from very high resolutions since optical carrier frequencies are much higher than RF signal bandwidths. The electrical system demonstrated here cannot resolve finer than approximately 0.1-ns features in a 0.6-ns window (permitting six resolution elements; hence, the authors' choice of digital bit-signaling for this demonstration). However, system resolution can be improved by choosing higher RF carrier frequencies. A carrier frequency of 15 GHz would result in 18 resolution elements assuming the same 0.6-ns window used here. This is made challenging because losses incurred in microstrips scale with $\sqrt{\omega}$, and an upper limit between 15–20 GHz is anticipated before attenuation becomes a problem. Using an EBG with negative chirp values (reflecting the higher lossier frequencies first) can help mitigate loss effects.

The authors wish to point out that the choice of frequencies in this demonstration was limited by available technologies, which are not state-of-the-art (e.g., $0.5\text{-}\mu\text{m}$ SiGe), computer simulation-time constraints, and available impulse generation equipment. Electronic time-stretch systems may achieve better resolution and time-bandwidth figures exceeding ten with broader-bandwidth multipliers and longer EBGs designed for higher carrier frequencies. In an estimate of what could be reasonably expected from the state-of-the-art, we note that analog multipliers with bandwidths of 23 GHz have been reported [16], and that the reference frequency sweep can be extended to larger bandwidths by using narrower impulses, with some commercially available impulse-forming networks now capable of forming ~ 15 -ps impulses. The authors believe the most limiting factor of the electronic implementation is that EBG microstrips with higher group-delay slopes and bandwidths would require, in general, more length. For example, targeting a 2-ns window of an RF signal of 8-GHz bandwidth (a time-bandwidth product of 16) would require a group-delay slope of greater than 1 ns/GHz and a corresponding microstrip length of approximately 48 cm according to (1) and the design equations laid out in [11]. Since raising the effective permittivity would mitigate this problem, the authors again anticipate the role that stripline EBG structures may have to play since they use true rather than effective permittivity. Stripline structures also offer true TEM-mode propagation (as opposed to quasi-TEM in microstrip), which is highly advantageous for building broadband directional couplers [18] and, thus, the authors suspect these couplers could be integrated directly into the EBG device design.

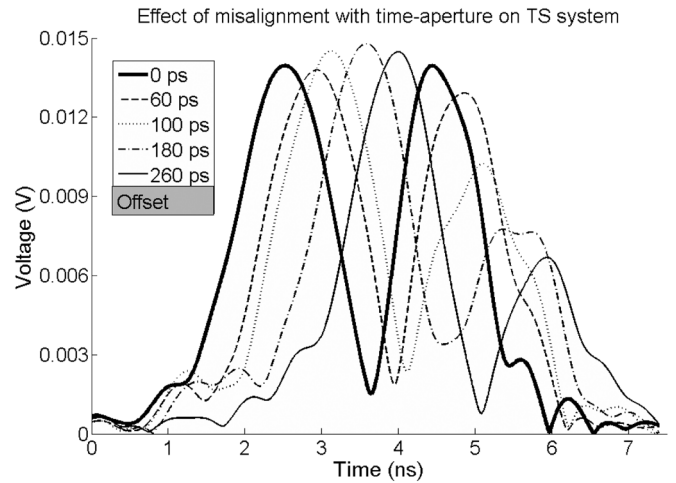


Fig. 9. Temporal misalignment with the time-aperture results in degraded quality of signal envelope. A 150-ps misalignment outside of the 600-ps aperture results in degradation of detected bit amplitude by over 50%.

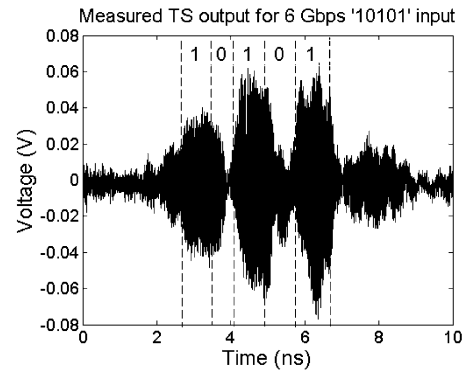


Fig. 10. Measured system output for a 6-Gb/s "10101" bit pattern of 0.82 ns. This bit pattern exceeds the rated 0.6-ns window length and one bit is noticeably attenuated and broadened.

C. Timing Issues

It is important in a time-stretch system that the dispersed input signal arrives at the mixer input at the same time as the reference frequency sweep to obtain the correct difference frequency. If part of the input signal is time shifted away from the ideal triggering case depicted in Fig. 3, two problems occur, which are: 1) there may be no component of the reference frequency sweep at the mixer input or 2) the mixer product will be frequency shifted and, thus, fall outside the passband of the subsequent dispersive device.

By keeping the reference pulse at a fixed time while advancing the input bit sequence in time, the demonstration system (0.6-ns window, "101" sequence) tolerates approximately 150 ps of temporal misalignment outside this window before one of the input "1" bits becomes approximately 50% attenuated, as shown in Fig. 9 using MATLAB to process the measured S -parameter data of the chirped EBGs. Similarly, we demonstrate in Fig. 10 a measured oscilloscope response to a 6-Gb/s bit pattern of "10101," which is 0.82 ns in length and, thus, is larger than the system's temporal aperture. As a result, one of the bits is "defocused" in this temporal imaging system, emerging broader and attenuated. Time-stretch systems are also

subject to aberrations due to departures from ideal quadratic phase behaviors, a detailed discussion of which can be found in [19].

D. Other Points of Comparison

Another point of comparison with optical systems is output signal detection, which must be achieved by extracting the envelope of a chirped-carrier signal. For systems employing signal conversion to the optical domain, this step is trivial due to high optical carrier frequencies (in terahertz) and the mere act of photodetection is sufficient to recover the desired signal envelope. This is not the case for an electrical time-stretch system in which a peak-detection or down-conversion scheme must be employed to recover the amplitude features of the signal on a one-shot basis.

It is also interesting to note the ability of optical time-stretch systems to entirely remove the first dispersive element of the system, and they can recast the magnification factor in terms of two dispersive elements related by an inequality rather than a precise equality, sometimes referred to as “simplified” temporal imaging [1], [20]. Electrical systems may not be able to benefit in this regard since one requirement of this simplified implementation is that the bandwidth at the output of the time lens should be much greater than the input bandwidth, and this would likely present a challenge for electronic systems in the context of practical analog multiplier design for UWB systems where input bandwidths are already large.

V. CONCLUSION

In this paper, we have reported on the first demonstration of a fully electronic implementation of a time-magnification system for bandwidths in the range of UWB systems. This has significant implications for improving the effective bandwidth of ADCs to accommodate the spectrum of UWB communication systems. The key development enabling this system is the chirped EBG structure, which is a broadband source of strong dispersion. We have demonstrated $5\times$ magnification of a 0.6-ns signal window with 8-GHz RF bandwidth. A system employing longer EBG structures, using current impulse generation equipment with the state-of-the-art in analog multiplier design, would be capable of achieving time-bandwidth products in excess of ten and would be comparable to what has been demonstrated using electrooptic modulation schemes, but without the costly optical components and with promising integration opportunities.

The authors will shortly follow up this study with an experimental demonstration of an electronic time-compression system to demonstrate the potential application of this technique for AWG applications in UWB communication technologies.

ACKNOWLEDGMENT

The authors gratefully acknowledge the assistance of M. Guttman, N. Kheder, and M. Nikolic, all with McGill University, Montréal, QC, Canada, for their role in the design and layout of the analog multiplier, as well as Dr. M. El-Gamal, McGill University, for his assistance providing access to test equipment.

REFERENCES

- [1] F. Coppinger, A. S. Bhushan, and B. Jalali, “Photonic time-stretch and its application to analog-to-digital conversion,” *IEEE Trans. Microw. Theory Tech.*, vol. 47, no. 7, pp. 1309–1314, Jul. 1999.
- [2] Y. Han and B. Jalali, “Photonic time-stretched analog-to-digital converter: fundamental concepts and practical considerations,” *J. Lightw. Technol.*, vol. 21, no. 12, pp. 3085–3103, Dec. 2003.
- [3] F. Coppinger, A. S. Bhushan, and B. Jalali, “Time magnification of electrical signals using chirped optical pulses,” *Electron. Lett.*, vol. 34, no. 4, pp. 399–400, Feb. 1998.
- [4] J. Azaña, N. K. Berger, B. Levit, and B. Fischer, “Broadband arbitrary waveform generation based on microwave frequency upshifting in optical fibers,” *J. Lightw. Technol.*, vol. 24, no. 7, pp. 2663–2675, Jul. 2006.
- [5] J. Chou, Y. Han, and B. Jalali, “Adaptive RF-photonic arbitrary waveform generator,” *IEEE Photon. Technol. Lett.*, vol. 15, no. 4, pp. 581–583, Apr. 2003.
- [6] J. Schwartz, J. Azaña, and D. V. Plant, “A fully electronic time-stretch system,” presented at the 12th Int. Antenna Technol. Appl. Electromagn. Symp., 2006.
- [7] W. J. Caputi, “Stretch: A time-transformation technique,” *IEEE Trans. Aerosp. Electron. Syst.*, vol. 7, no. 2, pp. 269–278, Mar. 1971.
- [8] B. Kolner, “Space-time duality and the theory of temporal imaging,” *IEEE J. Quantum Electron.*, vol. 30, no. 8, pp. 1951–1963, Aug. 1994.
- [9] P. Naulleau and E. Leith, “Stretch, time lenses, and incoherent time imaging,” *Appl. Opt.*, vol. 34, no. 20, pp. 4119–4128, Jul. 1995.
- [10] B. Kolner and M. Nazarathy, “Temporal imaging with a time lens,” *Opt. Lett.*, vol. 14, no. 12, pp. 630–632, Jun. 1989.
- [11] M. A. G. Laso, T. Lopetegi, M. J. Erro, D. Benito, M. J. Garde, M. A. Muriel, M. Sorolla, and M. Guglielmi, “Real-time spectral analysis in microstrip technology,” *IEEE Trans. Microw. Theory Tech.*, vol. 51, no. 3, pp. 705–717, Mar. 2003.
- [12] C. Bennett and B. Kolner, “Principles of parametric temporal imaging—Part I: System configurations,” *IEEE J. Quantum Electron.*, vol. 36, no. 4, pp. 430–437, Apr. 2000.
- [13] M. A. G. Laso, T. Lopetegi, M. J. Erro, D. Benito, M. J. Garde, M. A. Muriel, M. Sorolla, and M. Guglielmi, “Chirped delay lines in microstrip technology,” *IEEE Microw. Wireless Compon. Lett.*, vol. 11, no. 12, pp. 486–488, Dec. 2001.
- [14] M. J. Erro, M. A. G. Laso, T. Lopetegi, M. J. Garde, D. Benito, and M. Sorolla, “A comparison of the performance of different tapers in continuous microstrip electromagnetic crystals,” *Microw. Opt. Technol. Lett.*, vol. 36, no. 1, pp. 37–40, Jan. 2003.
- [15] B. Tzeng, C. Lien, H. Wang, Y. Wang, P. Chao, and C. Cheng, “A 1–17-GHz InGaP–GaAs HBT MMIC analog multiplier and mixer with broadband input-matching networks,” *IEEE Trans. Microw. Theory Tech.*, vol. 50, no. 11, pp. 2564–2568, Nov. 2002.
- [16] M. D. Tsai, C. S. Lin, C. H. Wang, C. H. Lien, and H. Wang, “A 0.1–23-GHz SiGe BiCMOS analog multiplier and mixer based on attenuation-compensation technique,” in *IEEE Radio Freq. Integr. Circuits Symp.*, 2004, pp. 417–420.
- [17] Y. Han, O. Boyraz, and B. Jalali, “Ultrawide-band photonic time-stretch A/D converter employing phase diversity,” *IEEE Trans. Microw. Theory Tech.*, vol. 53, no. 4, pp. 1404–1408, Apr. 2005.
- [18] D. Pozar, *Microwave Engineering*, 3rd ed. Hoboken, NJ: Wiley, 2005.
- [19] C. Bennett and B. Kolner, “Aberrations in temporal imaging,” *IEEE J. Quantum Electron.*, vol. 37, no. 1, pp. 20–32, Jan. 2001.
- [20] J. Azaña, N. K. Berger, B. Levit, and B. Fischer, “Simplified temporal imaging systems for optical waveforms,” *IEEE Photon. Technol. Lett.*, vol. 17, no. 1, pp. 94–96, Jan. 2005.



Joshua D. Schwartz (S’01) received the B.Eng in electrical engineering (with honors) from McGill University, Montréal, QC, Canada, in 2003, and is currently working toward the Ph.D. degree at McGill University.

He is currently with the Photonics Systems Group, McGill University. He has authored or coauthored over 12 publications and conference presentations. His research areas of interest include real-time microwave signal processing, EBG structures, and metamaterials.

Mr. Schwartz was the recipient of a 2003 British Association Medal as the top graduating student of his B.Eng program.



José Azaña (M'03) received the Ingeniero de Telecomunicación and Ph.D. degrees in optical signal processing from the Universidad Politécnica de Madrid (UPM), Madrid, Spain, in 1997 and 2001, respectively.

He recently joined the Institut National de la Recherche Scientifique (INRS)-Energie, Montréal, QC, Canada, where he is currently a Research Professor with the Ultrafast Optical Processing (UOP) Group. His research has resulted in over 50 publications in scientific and engineering journals.

Dr. Azaña is a member of the Optical Society of America (OSA). He has been recognized with several distinctions in both Spain and Canada.



David V. Plant (S'86–M'89–SM'05) received the Ph.D. degree in electrical engineering from Brown University, Providence, RI, in 1989.

Since 1993, he has been a Professor and member of the Photonic Systems Group, Department of Electrical and Computer Engineering, McGill University, Montréal, QC, Canada. In January, 2006, he became the Associate Dean of Research and Graduate Education. He is also a James McGill Professor (Tier I Canada Research Chair institutional equivalent).

Dr. Plant is an IEEE Distinguished Lecturer (2005–2007). He is a Fellow of the Optical Society of America. He is a member of Sigma Xi. He was the recipient of the 2006 IEEE Canada R. A. Fessenden Medal.